Interaction Between the Indian Ocean Dipole and ENSO Associated with Ocean Subsurface Variability

Hui Wang[1], Arun Kumar[1], and Raghu Murtugudde[2]
[1]Climate Prediction Center, NOAA/NWS/NCEP, College Park, Maryland
[2]ESSIC, University of Maryland, College Park, MD

1. Introduction

The Indian Ocean dipole (IOD) is an intrinsic coupled mode of variability in the tropical Indian Ocean. It has broad impacts on regional climate. An IOD index is defined as the difference between sea surface temperature (SST) anomalies averaged over the western Indian Ocean (WIO, 50°–70°E, 10°S–10°N) and eastern Indian Ocean (EIO, 90°–110°E, 10°S–Eq.). An important issue in the studies of IOD is the relationship between IOD and the El Niño-Southern Oscillation (ENSO) and the potential feedbacks from each other. Previous studies have shown that the development of IOD can be independent of ENSO, but ENSO may exert significant influence. In recent years, it has also been found that IOD can affect ENSO. Clearly, there exists an intimate interaction between IOD and ENSO but the detailed phenology of their mutual evolution has not been reported thus far.

Although a positive (negative) IOD tends to co-occur with El Niño (La Niña), the spatial-temporal covariations of these two major climate modes have not been well documented. Our earlier modeling study (Wang *et al.* 2016) documented the time evolution of IOD and the associated ocean subsurface variability in the absence of ENSO. The current study is aimed at examining the time evolution of IOD in the presence of ENSO and characterizing the interaction between IOD and ENSO. The present work complements our previous analysis by looking at the spatial-temporal covariations between IOD and ENSO, identifying any lead-lag relationships between them, and quantifying the influence of ENSO on IOD. This is done by analyzing a 500-year long fully coupled model simulation, which retains the ENSO variability (referred to as ENSO run hereafter), and comparing the results with a parallel 500-year simulation with the ENSO variability suppressed
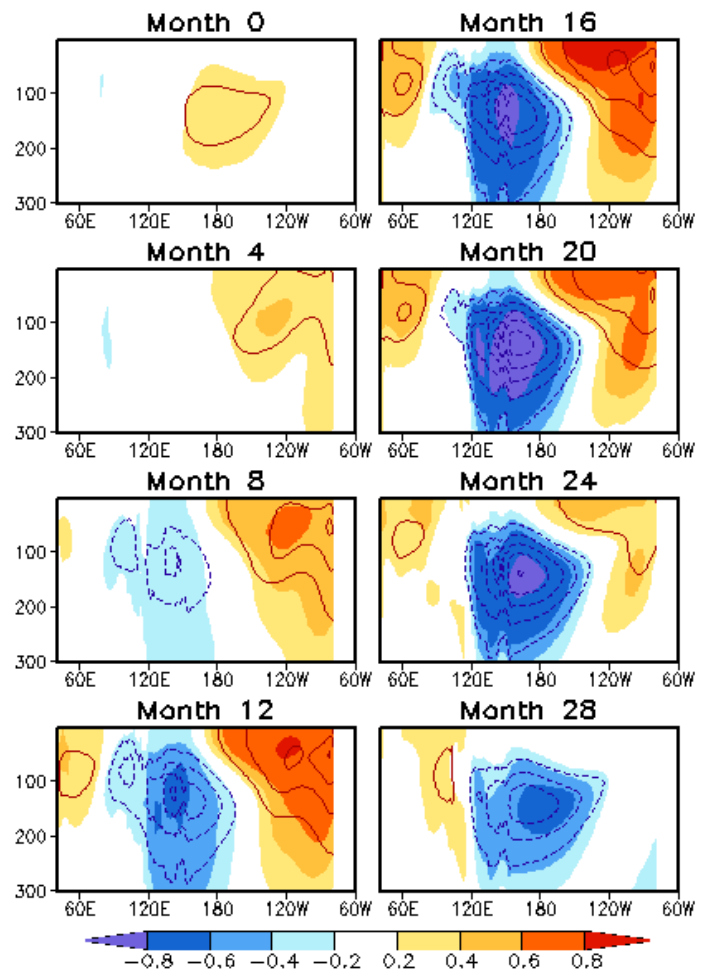

Fig. 1 Correlation (shading) and regression (contour) coefficients of monthly mean ocean temperature averaged over 10°S–5°N against the PC time series of the first EEOF from month 0 to month 28. Month 28 denotes ocean temperature lagging PC1 by 28 months. Contour interval is 0.25 K with negative values dashed and zero contours omitted.

Correspondence to: Hui Wang, Climate Prediction Center, NOAA/NWS/NCEP, 5830 University Research Court, College Park, MD; E-mail: hui.wang@noaa.gov

(daily SST nudged to its climatology in the tropical Pacific; referred to as no-ENSO run hereafter). The latter was analyzed in Wang *et al.* (2016) to characterize the spatial-temporal evolution of IOD in the absence of ENSO. The differences in the characteristics of IOD between the two simulations will indicate the impact of ENSO on IOD.   Both simulations were conducted with the NCEP CFS version 1 coupled model.

2. Covariations between IOD and ENSO

The spatial-temporal covariations between IOD and ENSO are examined by using the extended empirical orthogonal function (EEOF) method.   The EEOF analysis is based on the spatial-temporal covariance matrix of monthly mean ocean temperature from the last 480-year ENSO run averaged between 10°S and 5°N with a temporal window of 18 months.   The longitude–depth domain for the EEOF analysis is from 50°E to 180° over the tropical Indian Ocean and western Pacific and from the 5-m depth to the 225-m depth below the sea surface.

Figure 1 shows the first EEOF mode in the form of correlation and regression maps for ocean temperature averaged between 10°S and 5°N.   They are obtained by correlating and regressing the ocean temperature anomalies against the principal component (PC) time series of EEOF1 for ocean temperature lagging PC1 by 0 month to 28 months. This mode accounts for 31% of surface and subsurface temperature variance in the tropical Indian Ocean and western Pacific.

Fig. 2 Same as Fig. 1 but for the second EEOF.

The time evolution of EEOF1 begins with warm subsurface temperature anomalies in the tropical western Pacific (Fig. 1, month 0). From month 0 to 4, they propagate eastward along the thermocline and generate warm SST anomalies in the eastern and central Pacific, which leads to Bjerknes feedback and an El Niño. In the following months (months 8-16), the El Niño continues to grow with increases in SST and subsurface temperature anomalies. In the meantime, cold temperature anomalies develop in the tropical western Pacific, as well as in EIO while warm anomalies develop in WIO. The latter two form a positive IOD. During the decay phase of the El Niño (months 16-24), warm temperature anomalies in WIO move eastward and replace cold anomalies in EIO, nearly synergistically with the eastward propagating cold anomalies in the subsurface tropical Pacific. As a consequence, a basin-wide warming takes place in both the surface and subsurface tropical Indian Ocean, consistent with the processes of the tropical Indian Ocean surface and subsurface responses to El Niño found in previous studies. Figure 1 illustrates that the development of a positive IOD and its transition to a basin-wide warming in the tropical Indian Ocean are embedded in the evolution of an El Niño and thus lag the El Niño. EEOF1 reflects the IOD response to ENSO.

The second EEOF is shown in Fig. 2, which accounts for 16% of the surface and subsurface temperature variance. In month 0, there is an El Niño in the tropical Pacific and a positive IOD in the tropical Indian Ocean. Similar to EEOF1 (Fig. 1, months 16-24), the decay of the El Niño in EEOF2 is associated with the thermocline variability in the tropical Pacific and eastward propagating temperature anomalies in the tropical Indian Ocean, leading to a basin-wide mode (Fig. 2, months 8-16). In month 20, the tropical Pacific is characterized by a La Niña, whereas EIO is dominated by warm anomalies. In the following months, cold
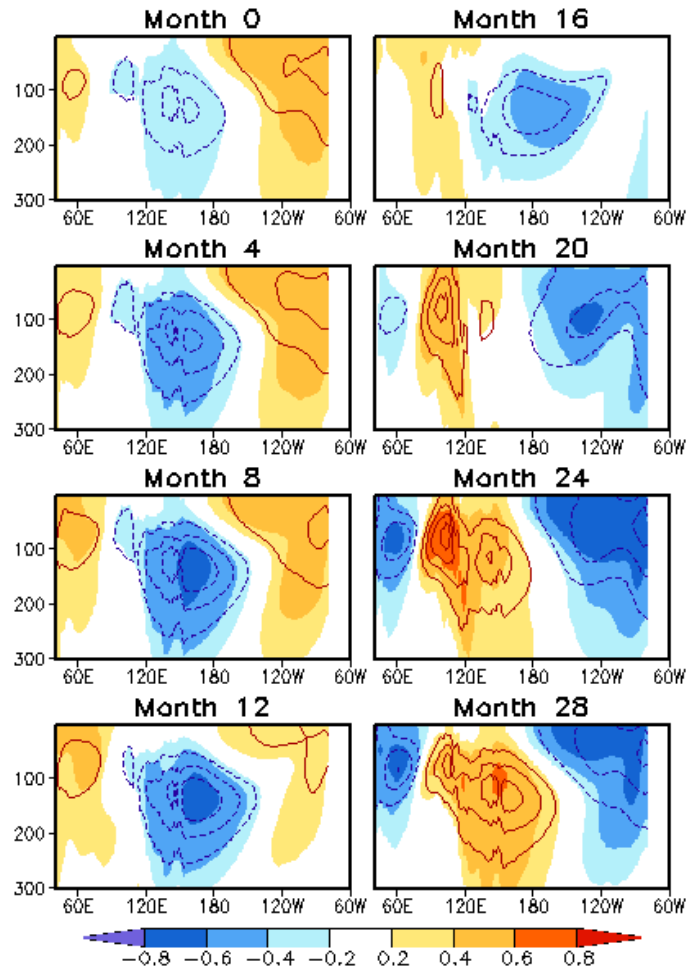
anomalies develop in WIO, leading to a negative IOD. Additionally, there are weak warm anomalies in the western Pacific in month 20 following the development of warm anomalies in EIO. These warm anomalies continue to intensify during months 20-28, shift eastward, and continue to prepare the deep tropical Pacific for the next El Niño. The warm anomalies in the surface and subsurface of the western Pacific come after the warm anomalies in EIO originating from WIO. This suggests that both the IOD and the following basin-wide mode lead the forthcoming El Niño.
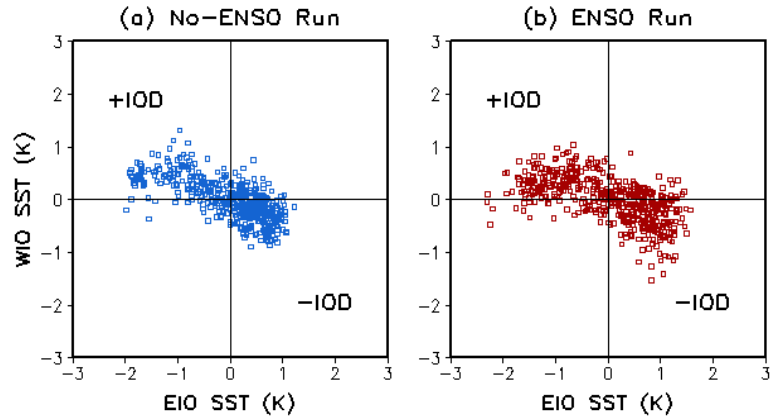

Fig. 3 Scatter plot of 480-year EIO SST versus WIO SST in SON for (a) the no-ENSO run and (b) the ENSO run.

The two leading EEOF modes capture the covariations between IOD and ENSO that are associated with tropical ocean subsurface variability. In both modes, there are strong links between surface and subsurface temperature anomalies. In the first mode, a positive IOD lags an El Niño. In the second mode, a positive IOD and a basin-wide mode lead the development of warm ocean temperature anomalies in the western Pacific and the occurrence of El Niño. The results suggest that the IOD and the basin-wide warming in the tropical Indian Ocean may be a response to El Niño, which in turn may help the development of El Niño. Their two-way interaction is further examined in the following two sections.

3. Impact of ENSO on IOD

A comparison of the power spectra of the IOD index between the ENSO run and no-ENSO run (not shown) suggests that ENSO significantly enhances the variability of IOD at interannual time scale. ENSO can also affect the intensity of IOD. Figure 3 shows the scatter plot of EIO SST anomaly versus WIO SST anomaly in September-November (SON), the peak season of IOD, for both the ENSO run and no-ENSO run. It is evident that the amplitudes of these SST anomalies are larger in Fig. 3b than in Fig. 3a, especially in the right lower quadrant during the negative IOD phase. Compared to the no-ENSO run, the SST variance in the ENSO run is enhanced by 42% and 25%, respectively, in the eastern and western poles of IOD. The variance of the IOD index is increased by 30%. The corresponding increases are 14% (eastern pole), 2% (western pole), and 6% (dipole) when IOD is in a positive phase. In contrast, they are 55%, 50%, and 52% when IOD is in a negative phase. Therefore, the ENSO impact on the IOD intensity is larger for the eastern pole than for the western pole, and is stronger during a negative IOD event than during a positive event. The results reveal an asymmetry of the ENSO influence between the positive and negative IOD phases.

4. Influence of IOD on ENSO prediction

The impact of IOD on ENSO should be manifest in its influence on the skill of ENSO prediction. Figure 2 demonstrates that the evolution of EEOF2 involves eastward propagation of warm temperature anomalies from WIO, followed by the development of warm subsurface temperature anomalies in the western tropical Pacific which in turn leads to an El Niño. The processes provide a physical basis for using SST anomaly in WIO as a predictor for ENSO prediction. To demonstrate the feasibility of this claim, a linear regression model is employed to statistically forecast winter seasonal mean (December-February, DJF) Niño 3.4 SST. The forecasts are cross-validated and compared with statistical forecasts using warm water volume (WWV) as a predictor, defined as the volume of water warmer than 20°C in the tropical Pacific (120°E-80°W, 5°S-5°N) derived from TAO moorings, as well as the CFSv2 dynamical seasonal forecasts.

Figure 4 shows the forecast skills assessed by anomaly correlations between the predicted and observed Niño 3.4 SST over 1983-2010, the CFSv2 hindcast period. Both predictors, namely, WIO SST and WWV, are derived from preseason observations. To predict DJF Niño 3.4 SST, WIO SST and WWV of each month from the January of previous year to the November of current year are used as an input for the linear-

regression forecast model, corresponding to lead times from 22 months to 0 month (Fig. 4, x-axis labels). The CFSv2 only provides 9-month lead forecasts, resulting in the DJF Niño 3.4 SST forecasts with lead times from 6 months (initialized in May) to 0 month (initialized in November).

Fig. 4 Anomaly correlation skills of CFSv2 dynamical forecast (black) and statistical forecasts using one predictor (blue for WWV; red for WIO SST) and two predictors (WWV + WIO SST, green) for DJF Niño 3.4 SST with lead times from 22 months to 0 month, corresponding to forecasts made from January of previous year to November of current year (Jan– to Nov0 with – and 0 for previous year and current year, respectively). Solid (dash) gray line denotes the threshold of the anomaly correlation at the 99% (95%) significance level.

The CFSv2 has the highest forecast skill at all available lead times (Fig. 4, black line). The skill of the statistical forecasts based on WWV (blue line) is lower than the dynamical forecasts, but the anomaly correlations are above the 99% significance level (0.48, solid gray line) at 0- to 10-month leads. There is a sharp decrease in the anomaly correlation at the 12-month lead, beyond which no skillful forecasts are found. The maximum lead of 12 months is likely determined by the time needed for subsurface temperature anomalies from the tropical western Pacific to cross the Pacific basin and reach the sea surface in the tropical eastern Pacific. When using the WIO SST as a predictor (red line), skillful forecasts are found at either a short lead time of 0 month (above the 99% significance level) or longer leads of 12–16 months (above the 95% significance level). The former is associated with the co-occurrence of IOD and ENSO, whereas the latter is attributed to the signal of warm WIO SST anomalies appearing well ahead (> 1 year) of El Niño (Fig. 2). The skill of the WIO SST-based forecasts is lower than those of the CFSv2 and the WWV-based forecasts, but the lead time of skillful forecasts with the WIO SST is longer than the other two.

When using both WIO SST and WWV as predictors, the forecast skill (Fig. 4, green line) is comparable to that based solely on WWV (blue line) at lead times from 0 to 10 months, but is significantly improved at longer leads. Figure 4 suggests that for the ENSO prediction, the statistical forecast based on WWV can extend the limit of lead time of the dynamical forecast from 6 months to 10 months. Using the WIO SST as an additional predictor can further extend the lead times of skillful forecasts up to 13 (15) months at the 99% (95%) significance level.

5. Conclusions

The interaction between IOD and ENSO is examined using coupled global climate model simulations. The covariability of IOD and ENSO is analyzed by applying the EEOF method to the surface and subsurface ocean temperatures in the tropical Indian Ocean and western Pacific. The first EEOF mode shows the evolution of IOD that lags ENSO, whereas the second mode exhibits the transition from a dipole mode to a basin-wide mode in the tropical Indian Ocean that leads ENSO. Both modes have high loadings in the tropical ocean subsurface. The lead-lag relationships between IOD and ENSO suggest a two-way interaction between them. A comparison between two 500-year model simulations with and without ENSO suggests that ENSO can enhance the variability of IOD at interannual time scale. The influence of ENSO on the IOD intensity is larger for the eastern pole than for the western pole, and is stronger in a negative IOD phase than in a positive phase. The influence of IOD on ENSO is demonstrated by the improvement of ENSO prediction with a linear regression forecast model when considering SST in the western pole as an ENSO precursor. The improvement of the ENSO forecast skill is found not only at a short lead time (0 month) but also at long leads
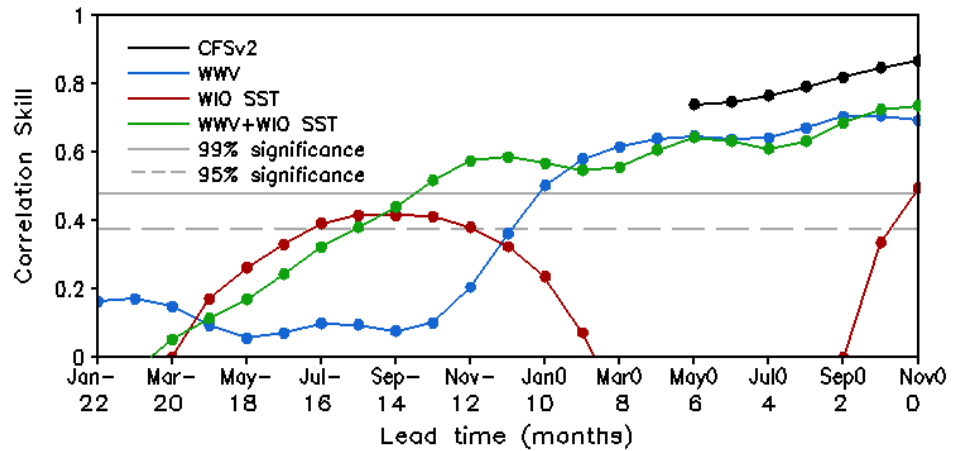
(10-15 months). The eastward propagation of surface and subsurface temperature signals from WIO that precede the development of heat content anomaly in the tropical western Pacific is the key for extending the lead time for ENSO prediction. Our results are consistent with previously reported findings but add finer points to the mechanisms of ENSO-IOD interactions and improve the predictive understanding of the monsoon-IOD-ENSO system. Forecast experiments with CFS are underway to quantify the impact in the full coupled framework so that the details of the oceanic tunnel and the atmospheric bridge of this active partnership between IOD and ENSO can be fully exploited.

References

Wang H., R. Murtugudde, and A. Kumar, 2016: Evolution of Indian Ocean dipole and its forcing mechanisms in the absence of ENSO. *Clim. Dyn.*, **47,** 2481–2500.